Industrial Waste Derived Separators for Zn-Ion Batteries Achieve Homogeneous Zn(002) Deposition Through Low Chemical Affinity Effects

Chengwu Yang[1], Pattaraporn Woottapanit[1], Yilei Yue[1], Sining Geng, Jin Cao, Xinyu Zhang, Guanjie He*, Jiaqian Qin**

Dr. C. Yang, P. Woottapanit, Dr. J. Qin

Center of Excellence in Responsive Wearable Materials, ~~Center of Excellence on Advanced Materials for Energy Storage~~

Metallurgy and Materials Science Research Institute

Chulalongkorn University

Bangkok 10330, Thailand

Email: jiaqian.q@chula.ac.th

Dr. C. Yang, Dr. Y. Yue, S. Geng, Prof. X. Zhang

State Key Laboratory of Metastable Materials Science and Technology

Yanshan University

Qinhuangdao 066004, P. R. China

Email: xyzhang@ysu.edu.cn

Dr. J. Cao

College of Materials and Chemical Engineering

China Three Gorges University

Yichang, Hubei 443002, China

Dr. G. He

Christopher Ingold Laboratory

Department of Chemistry

University College London

London WC1H 0AJ, UK

Email: g.he@ucl.ac.uk

[1] These authors contributed equally to this work.

Keywords: zinc-ion batteries, cellulose, fly ash, desolvation energy barrier, stable Zn

anode

Abstract

Designing a cost-effective and multifunctional separator that ensures dendrite-free and stable Zn metal anode remains a significant challenge. Herein, we present a multifunctional cellulose-based separator consisting of industrial waste-fly ash particles and cellulose nanofiber using a facile solution-coating method. The resulting fly ash-cellulose (FACNF) separators enable a high ion conductivity (5.76 mS cm^{-1}) and low desolvation energy barrier of hydrated Zn^{2+}. These features facilitate fast ion transfer kinetics and inhibit water-induced side reactions. Furthermore, experimental results and theoretical simulations confirm that the presence of fly ash particles in FACNF separators effectively accommodate the preferential deposition of Zn(002) planes, due to the weak chemical affinity between Zn(002) plane and fly ash, to mitigate dendrite formation and growth. Consequently, the utilization of FACNF separators causes an impressive cycling performance in both Zn||Zn symmetric cells (1600 h at 2 mA cm^{-2}/1 mAh cm^{-2}) and Zn||$(NH_4)_2V_{10}O_{25}$ (NVO) full cells (4000 cycles with the capacity retention of 92.1% at 5 A g^{-1}). Furthermore, the assembled pouch cells can steadily support digital thermometer over two months without generating gas and volume expansion. This work provides new insights for achieving crystallographic uniformity in Zn anodes and realizing cost-effective and long-lasting aqueous zinc-ion batteries.

1. Introduction

Lithium-ion batteries (LIBs) as a new type of secondary energy system have been widely applied in portable electronics and electric vehicles, dominating the rechargeable energy supply market.[1, 2] However, high cost of industrial manufacture, high risk of thermal runaway and low abundance of lithium resources make them unfavorable for the large-scale energy storage applications.[3-6] Recently, Aqueous zinc-ion batteries (AZIBs) have been considered as one of the most promising next-generation high-density energy storage systems due to its cost-effectiveness, environmental friendly nature, high safety and theoretical capacity (820 mAh g^{-1}).[7, 8] Nevertheless, Zn metal anode due to its high activity in aqueous electrolyte is inevitably

confronted with critical issues, including dendrite growth, surface corrosion and hydrogen evolution reaction (HER), causing the low Coulombic efficiency and fast battery failure, as a result, presenting a challenge for the commercialization of AZIBs.

Heretofore, various techniques with multifunctional materials have been developed to surmount the above issues, such as solid-electrolyte interfacial (SEI) modification, electrolyte engineering, novel separator design and anode structural optimization.[9-15] Among them, separator design is the simple and effective way to handle the drawbacks of AZIBs. Hydrophilic polyolefin, filter paper and glass fiber usually work as the commercial separator in AZIBs,[16-19] but they are unable to resist the heterogeneous Zn deposition and parasitic reactions during Zn deposition/dissolution process due to their sluggish and inhomogeneous ion transportation. Besides, the high cost of these separators makes them hard to hold both low cost and high energy density per unit cell. Currently, researchers have reported many novel separators with highly efficient ability to stabilize Zn anodes in AZIBs, for examples, GO/cellulose,[20] $Ti_3C_2T_x$ MXene/glass fiber,[21, 22] $NaZnF_3$ and Nafion decorated cotton,[23] UiO-66 MOF/glass fiber[24] and PVDF@PDF nanofibrous,[25] etc. However, the tedious fabrication routes of the developed separators as well as the exorbitant spending on chemical materials greatly restrict their practical applications. Therefore, taking the requirements of commercializing AZIBs into consideration, the major problems that the ideal separators urgently need to solve in AZIBs are as below:[26-29] (1) The formation and growth of Zn dendrite on the Zn metal surface will lead to the failure of separators and the short-circuits of battery. (2) Surface corrosion, passivation and HER on Zn anodes cannot be inhibited by the separators, which could reduce the energy density of AZIBs and cause battery self-discharge. (3) Microstructure and surface chemistry of separators cannot afford high ionic conductivity and ion mobility number, which could lower ion/charge transfer kinetics and eventually worsen battery performances including capacity and cycling stability. (4) The fragile and expensive separators for AZIBs raise the fabrication cost of batteries. Hence, high-performance and low-cost separators are essential to produce batteries with high capacity, safety and long working life.

Fly ash, mainly consisting of quartz (SiO_2) and mullite (Al_2O_3), is an industrial waste generated from the combustion of coal.[30, 31] Owing to the enrichment of toxic trace element and its resistance to degradation, fly ash is recognized as an environmental contaminant. As coal consumption continues to rise, the disposal of the resulting fly ash has become an increasingly challenging issue worldwide. Fly ash particles are commonly used in cement industry, as well as the production of porcelain and glass, and for the treatment of gas and water due to their high plasticity and good thermostability.[32-34] However, their applications in the field of energy storage systems are still rarely reported. Thereby, to tackle the crux of AZIBs and rationally utilize fly ash particles, we designed a composite material comprising fly ash and cellulose nanofiber (FACNF) as the separator for AZIBs. This separator offers remarkable advantages of low cost (¥18.57 /m^2, compared with the popular glass fiber separator of ¥1900 /m^2), high thermal stability and superior flexibility. Through the experimental results and theoretical simulation, FACNF separators can not only improve the ion transfer kinetics and minimize Zn^{2+} desolvation energy barrier to curb undesirable water-involved side reactions, but also facilitate the preferential deposition of Zn(002) plane for the creation of a dendrite-free and stable Zn anode. Consequently, Zn||Zn symmetric cells incorporating FACNF separator achieve exceptional cycling lifespans of 1600 h at 2 mA cm^{-2}/1 mAh cm^{-2} and 550 h at 5 mA cm^{-2}/2.5 mAh cm^{-2}, surpassing those observed in cells with CNF. Moreover, the Zn||NVO full cell with FACNF separators also displays a higher discharge capacity and cycling stability.

2. Results and discussion

Figure 1a schematically illustrates the fabrication process of cost-efficient FACNF separators. The recycled fly ash microspheres and cellulose nano fiber dispersion were mixed in DI water, then casted on a glass substrate and dehydrated overnight. The digital photographs in Figure 1b display the prepared FACNF separator with the large size of 22 cm × 14 cm. Even undergone curling, folding, kneading, and then recovering states, the FACNF separator maintains the intact structure without any holes, indicating the excellent flexibility and machinal strength of FACNF separator. Based on the rate capabilities of Zn||Zn symmetric cells (Figure S1), the FACNF separator with a mass

fraction of fly ash of 20% generates the lowest voltage hysteresis during the whole process of increasing current density from 0.5 to 5 mA cm^{-2}, thus the optimal mass fraction of fly ash was determined as 20%. X-ray diffraction (XRD) patterns of fly ash, CNF and FACNF in Figure S2 indicate the successful preparation of FACNF separator. Scanning electron microscopy (SEM) and energy dispersive spectrometer (EDS) images of fly ash microspheres show the average diameter of 3.96 μm with the elemental composition of Si, Al, and O (Figure 1c and Figure S3). The pristine CNF separator exhibits a poriferous and rough microstructure with the membrane thickness of 53 μm (Figures 1d and S4a), while the FACNF separator expresses smooth and compact surfaces and slightly increases the thickness to 63 μm (Figure S4b). Such favorable structure of FACNF separator causes a lower water contact angle of 28.1° with higher wettability and hydrophilia than CNF (water contact angle of 44.8°) (Figure S5). Furthermore, the FACNF has a higher electrolyte uptake of 152.3% than that of CNF (84.5%). The thermal stabilities of CNF and FACNF separators were detected via thermogravimetric-differential thermal analysis (TG-DTA) under air atmosphere with the ramping rate of 10 ℃·min^{-1}. As shown in Figure 1g, the CNF separator initiates the rapid mass loss and decomposition when heated to 241 ℃, ascribing to dehydroxylation reaction in cellulose molecular chain.[35, 36] For the FACNF separator, the decomposition temperature of cellulose shows a redshift to 258 ℃, indicating the positive effect of fly ash on improving thermal stability. The filler of fly ash into CNFs can also modify the Zn^{2+} reaction kinetics on Zn anodes. The FACNF separator presents Zn^{2+} transfer number of 0.77 and ionic conductivity of 5.76 mS cm^{-1}, almost two and nine times respectively higher than that of CNF (0.45, 0.68 mS cm^{-1}, respectively), implying better electrochemical performances and Zn^{2+} ion diffusion abilities.[37] Figure 1h shows a Radar chart to compare the key parameters of CNF and FACNF, including cost, thermostability, water contactor angle and Zn^{2+} transference number, etc.

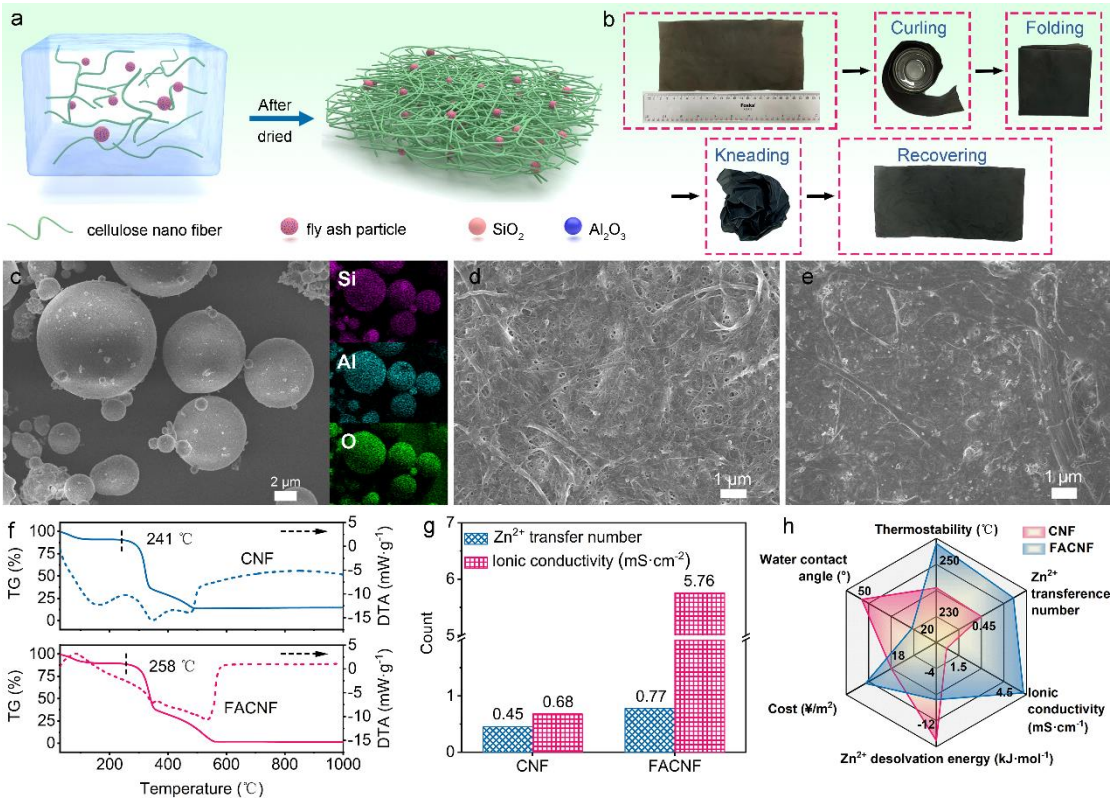

Figure 1. (a) The fabrication process of FACNF separators. (b) The digital photographs of FACNF separators under different states (curling, folding, kneading and recovering). (c) SEM image of fly ash microspheres with the elemental mapping. SEM images of (d) CNF and (e) FACNF separators. (f) TG-DTA curves and (g) Zn^{2+} transfer number and ionic conductivity of CNF and FACNF. (h) Radar chart of overall comparison of CNF and FACNF.

To investigate Zn^{2+} deposition behaviors affected by CNF and FACNF separators, the surface morphology of Zn anodes after plating was observed. As shown in Figure 2a-2c, after Zn plating with a capacity of 5 mAh cm^{-2}, the Zn anode of symmetric cell with the CNF separator exhibits irregular flake-like dendrite aggregation on the surface, caused by the uneven internal electric field distribution and Zn^{2+} flux density,[38] which will turn into large dendrites and finally result in the internal short circuits and battery failure. The surface of Zn anode with FACNF separators remains a homogeneous and dense morphology without any Zn clusters and dendrite protrusions, illustrating that the FACNF separator can promote a uniform electrochemical Zn deposition (Figure 2d-2f). In situ optical images of Zn deposition on Zn anodes were collected to visually

investigate the Zn deposition behavior under CNF and FACNF separator. For CNF separators, obvious Zn protrusions appear on the surface after plating 10 min and rapidly grow to large dendrite in the later 20 min (Figure 2g). As a comparison, when using FACNF separator, there is a smooth interface on the Zn anode without any observed Zn clusters and protrusions, indicating that the FACNF separator can homogenize Zn nucleation and subsequent Zn deposition, realizing the dendrite-free Zn anode (Figure 2h). The XRD patterns of Zn anodes after deposition were also obtained and shown in Figure 2i. The diffraction peak intensity of Zn(002) plane is weaker than Zn(101) plane with a low intensity ratio of Zn(002) to Zn(101) (0.77) when using CNF separators, reflecting that Zn^{2+} ions incline to vertically stack on the surface via Zn(101) plane and form the Zn dendrite. On the contrary, using FACNF separator leads to a Zn(002) dominant crystal orientation and a higher Zn(002)/Zn(101) intensity ratio of 1.63, meaning that Zn^{2+} ions preferentially deposit in parallel Zn surface direction.[39, 40]

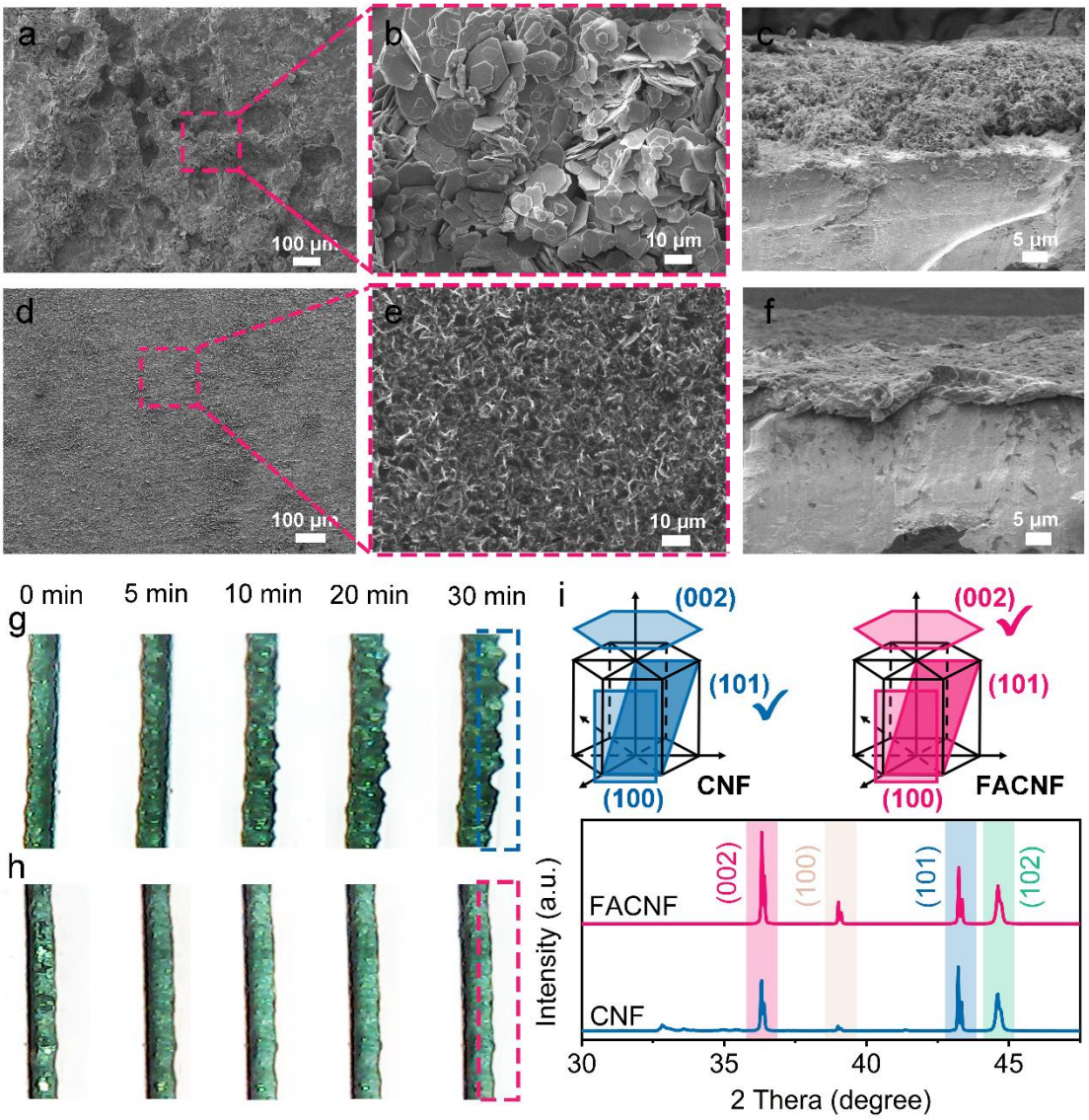

Figure 2. SEM images of Zn anodes after depositing the Zn with the areal capacity of 5 mAh cm^{-2} using (a-c) CNF and (d-f) FACNF separators. Confocal scanning microscope images of Zn anodes after deposition under (e) CNF and (f) FACNF separators. In situ optical images of Zn deposition on Zn anodes with (g) CNF and (h) FACNF. (i) XRD patterns of Zn anodes after deposition.

To certify the advantages of the FACNF separator in terms of the stability and reversibility of Zn deposition/dissolution, the electrochemical performance tests of Zn||Cu asymmetric cell and Zn||Zn symmetric cell using different separators were conducted. Figure 3a displays the cyclic voltammetry (CV) curves of Zn||Cu cells using CNF and FACNF separators. Notably, FACNF separator generates higher peak currents of cathodic and anodic loops and a smaller Zn nucleation overpotential on the Cu foil

(measured by the voltage-stable window between the gap of a and b points) compared with those with CNF separators, indicating a narrowed Zn deposition barrier of FACNF separator.[41] Such result is also demonstrated by the discharge voltage-time profiles at 1 mA cm^{-2}/3 mAh cm^{-2} (Figure 3b). The Zn nucleation overpotential of Zn||Zn cells with the CNF separator (160 mV) shows an almost twice higher than that with the FACNF separator (82 mV). In virtue of the improved nucleation kinetics and anticorrosion ability and uniform Zn deposition effect endowed by FACNF separators, a higher Coulombic efficiency (CE) of 99.2% in Zn||Cu cell is achieved after 250 cycles at 2 mA cm^{-2}/1 mAh cm^{-2} (Figure 3c). However, the CE value of CNF separators abruptly fluctuates after 10 cycles, due to the poor reversibility of Zn deposition/dissolution. Moreover, compared with CNF, the FACNF separator causes a lower overpotential and overlapped with voltage-potential curves at the selected cycles of Zn||Cu cells, further elucidating a better cycling stability and highly-reversible Zn deposition/dissolution behavior by FACNF separators (Figure S6).

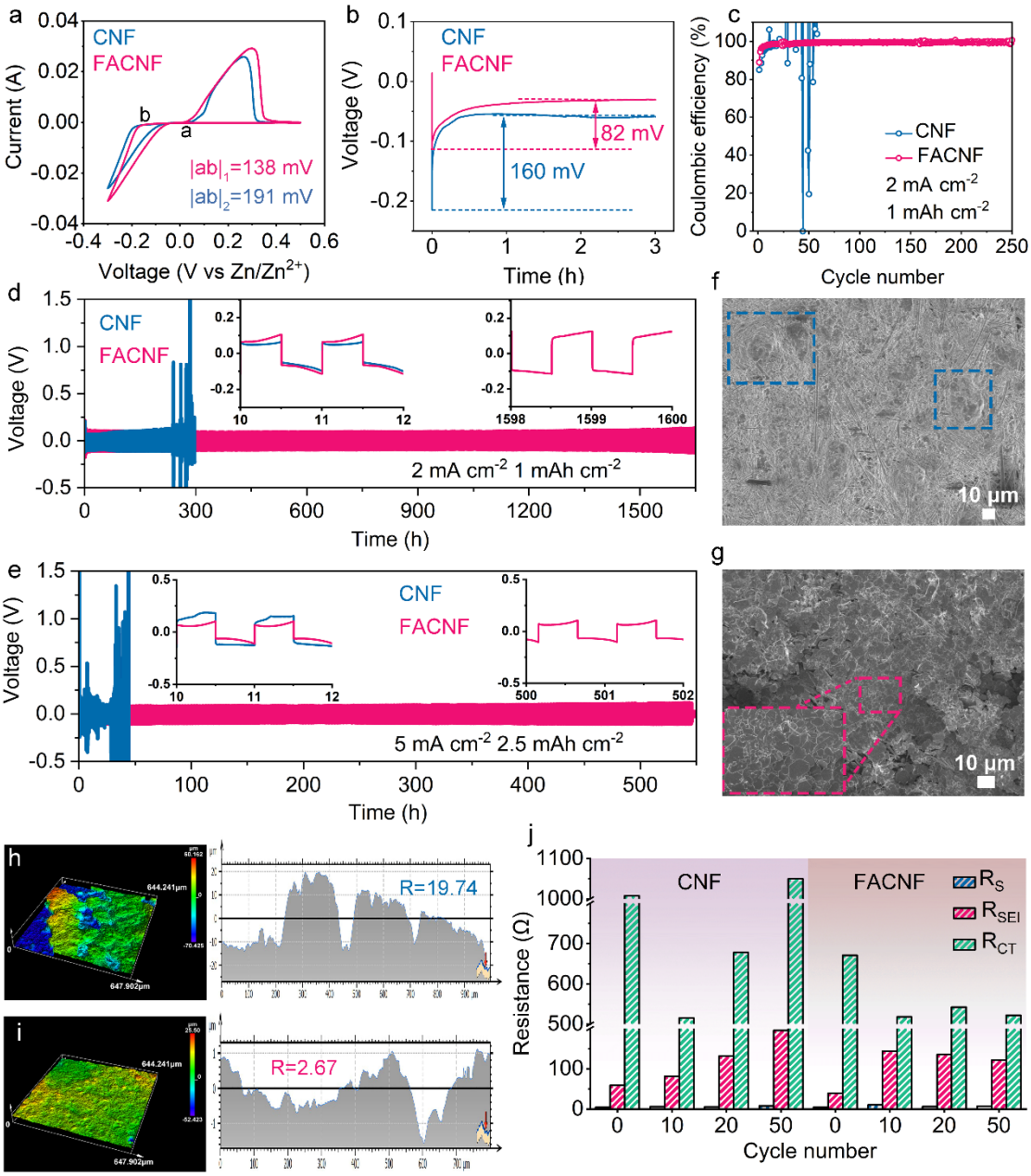

Figure 3. (a) CV curves of Zn||Cu with CNF and FACNF separators. (b) The discharge voltage-time profiles of Zn||Zn with CNF and FACNF separators at 1 mA cm^{-2}/3 mAh cm^{-2}. (c) The Coulombic efficiency of Zn||Cu with CNF and FACNF separators at 2 mA cm^{-2}/1 mAh cm^{-2}. The charge-discharge cycling performances of Zn||Zn with CNF and FACNF separators at (d) 2 mA cm^{-2}/1 mAh cm^{-2} and (e) 5 mA cm^{-2}/2.5 mAh cm^{-2}. SEM images of Zn anodes after cycling using (f) CNF and (g) FACNF separators. The confocal images of Zn anode with (h) CNF and (i) FACNF after cycling. (j) The resistances (R_s, R_{SEI} and R_{CT}) of Zn||Zn after cycling different times.

Figure 3d shows the long-term charge-discharge cycling performance of Zn||Zn

symmetric cells at 2 mA cm^{-2}/1 mAh cm^{-2}. The Zn||Zn cell with CNF presents an acute voltage vibration when cycling for 250 h, which can impute to dendrite growth and the occurrence of water-induced side reactions causing the accumulation of by-products and eventually increasing internal electrical resistance and sluggish ion/charge transport kinetics.[42] In comparison, the cell with FACNF can work steadily up to 1600 h with lower voltage hysteresis. Even increasing the applied current density and cycling capacity to 5 mA cm^{-2}/2.5 mAh cm^{-2}, the FACNF separator still affords a stable and long cycling capability of 550 h, compared with the CNF separator generating undulatory voltage profile within the whole cycling process (Figure 3e). Moreover, the cycling performance of Zn||Zn cells with FACNF separators is also better than with SiO_2-CNF (SOCNF) and Al_2O_3-CNF (AOCNF) separators (Figure S7). The morphology of Zn anodes after cycling was observed to disclose the root cause of the different cycling stability between CNFs and FACNFs. A mass of Zn dendrites as well the inlay of cellulose nanofiber are arisen on the surface of Zn anodes when using CNF separators (Figure 3f), whereas the FACNF separator brings a homogenous Zn(002) deposition layer without any dendrite formation (Figure 3g). Additionally, confocal scanning microscope images of Zn anodes further show significant differences between CNF and FACNF separators (Figures 3h and 3i, respectively), in which a flat Zn plating layer with smaller surface roughness (R = 2.67) is enabled by FACNF separators compared with the severe Zn dendrite and steep surface (R = 11.30) of CNF separators. EIS curves of Zn||Zn cells with CNF and FACNF separators at various cycles are shown in Figure S8 and the equivalent resistance values are listed in Figure 3j. The utilization of FACNF separators grants a much smaller SEI resistance (R_{SEI}, 39.3 Ω) and ion/charge transfer resistance (R_{CT}, 670.8 Ω) in the initial state than the CNF separator (59.0 and 1008 Ω, respectively). Remarkably, different from the gradual increment in R_{SEI} and R_{CT} of the CNF, the FACNF keeps a similar R_{SEI} and R_{CT} after different cycles, which ascribes to the homogeneous Zn deposition and suppressed side reactions during cycling processes.[37]

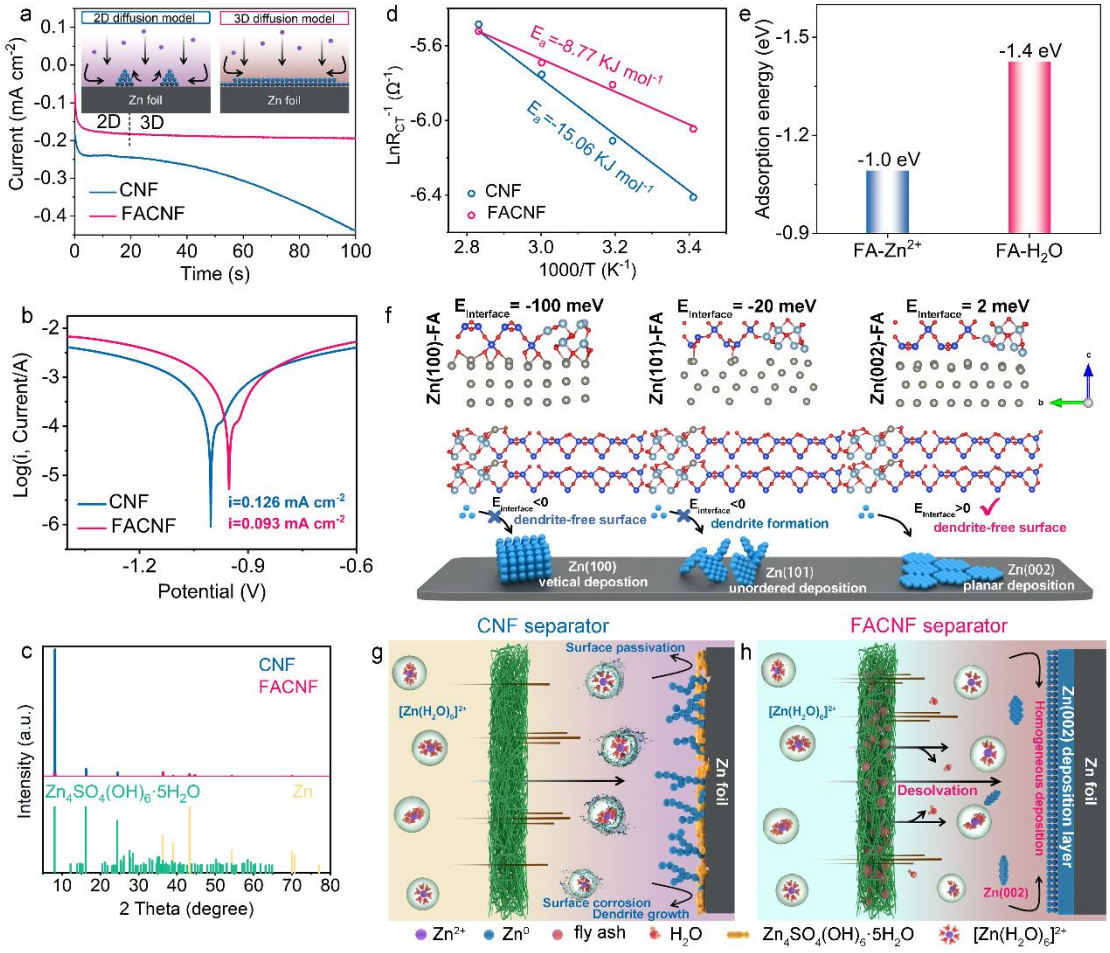

Figure 4. (a) CA curves and (b) Tafel curves of Zn anode using CNF and FACNF separators. (c) XRD patterns of Zn anodes after cycling. (d) The calculated desolvation energy of Zn^{2+}. (e) Calculated adsorption energies of Zn^{2+} and water molecules on fly ash. (f) The interface energy of Zn(100), Zn(101) and Zn(002) on fly ash particles with schematic illustration of Zn planes deposition on Zn anodes. The proposed possible mechanisms of (g) CNF and (h) FACNF for stable Zn anodes.

Chronoamperometry (CA) measurements were performed at the applied potential of 0.15 V to explore Zn nucleation and deposition mechanism.[43, 44] As seen from Figure 4a, CA curve shows that the current using CNF separator continuously reduces within the whole testing time of 100s, presenting the typical 2D diffusion model that can force Zn^{2+} ions to form large particles at high energy surface and further induce a rough deposition.[45] However, FACNF separator produces a quickly steady current after a short 2D diffusion of 20s, meaning the durable 3D diffusion process after Zn nucleation. Through this process, the Zn^0 nucleus reduced from Zn^{2+} ions could directly

absorb on the anode surface, preventing 2D diffusion and realizing homogeneous Zn deposition.[46] The anti-corrosion capability of the Zn anode was evaluated *via* Tafel curves (Figure 4b). The FACNF separator displays a lower exchange current density of 0.093 mA cm^{-2} than that of CNF separator (0.126 mA cm^{-2}), suggesting the alleviated corrosion activity of Zn anodes. In the linear sweep voltammetry (LSV) measurements (Figure S9), the lower onset potential of HER (-1.11 V) for the cells with FACNF separators than that with CNF separators (-1.07 V) at -10 mA cm^{-2} further suggests that surface corrosion and water-induced side reactions are effectually hindered by FACNF separators. The surface composition on Zn anodes after charge-discharge cycles was detected and the XRD patterns are shown in Figure 4c. The Zn anode of CNF separator exhibits intense diffraction peaks of $Zn_4SO_4(OH)_6{\cdot}5H_2O$ (PDF#39-0688) byproduct attributed to the serious side reactions, whereas there is a negligible diffraction peak of side reaction products observed in the Zn anode with FACNF separators, which directly demonstrates that the FACNF separators can improve anti-corrosion property and postpone the onset potential of side reactions.

The transfer and activation energy (E_a) of Zn^{2+} ions near the surface of Zn anodes were calculated via assessing the ion/charge transfer resistance (R_{CT}) at different temperatures. The Zn||Zn symmetric cell with FACNF has a smaller R_{CT} in comparison with that with CNF at all temperatures, reflecting the increment in the ion/charge transfer kinetics due to its higher ion transfer number and conductivity (Figure S10).[47] As calculated in Figure 4d, the higher Ea of 15.06 kJ mol^{-1} on CNF indicates the insurmountable energy barrier of Zn^{2+} desolvation. On the contrary, the E_a of FACNF is reduced to 8.77 kJ mol^{-1}, demonstrating a smaller desolvation energy barrier of hydrated Zn^{2+} and the accelerated reaction kinetics on the Zn anode surface regulated by FACNF. The adsorption energies of Zn^{2+} ion and water molecules on fly ash were calculated by density functional theory (DFT) calculations (Figure. 4e). Fly ash particles deliver a higher water adsorption energy than Zn^{2+} ions, implying a stronger interaction among water molecules and fly ash particles, which further proves that the fly ash particles can promote the desolvation of hydrated Zn^{2+}.[48, 49] The interaction between Zn crystal plane and fly ash was also revealed by DFT calculations. As shown

in Figure 4f, the interface energies between Zn(100) plane and fly ash as well as between Zn(101) plane and fly ash are -100 meV and -20 meV, respectively, indicating that fly ash particles have high chemical affinity toward Zn(100) and Zn(101) planes.[50] Such chemical affinity between them can restrain the Zn^{2+} transport from the electrolyte to form Zn(100) and Zn(101) planes during Zn deposition process, leading to an unfavorable crystal plane growth along Zn(100) and Zn(101). Conversely, the interface energy between Zn(002) and fly ash shows a positive value of 2 meV, signifying a negligible chemical interaction, which can support more Zn^{2+} for the preferable growth along Zn(002) plane. The DFT calculations further confirm that the FACNF separator can benefit the uniform and dendrite-free Zn deposition, which is consistent with the SEM and XRD results.

The Zn^{2+} transportation behavior and deposition mechanism based on CNF and FACNF separator was summarized. As depicted in Figure 4g, for CNF separator, owing to the inherent property of Zn metal in acidic electrolytes and the sluggish ionic conductivity of CNF separators, the Zn anode would undergo continuous side reactions, including surface corrosion and passivation and HER, during periodic Zn deposition/dissolution and the uneven Zn nucleation process could speed up the dendrite growth and “tip effect”, eventually resulting in the battery short circuit and failure.[51, 52] As for FACNF separators, the resultant stable and dendrite-free Zn anodes can be ascribed to three aspects (Figure 4h): the high ionic conductivity and Zn^{2+} transfer number from the FACNF separator can improve the ion deposition kinetics and uniformize Zn nucleation.[53] In addition, the strong interaction between fly ash particles and water molecules effectively guarantees a rapid desolvation process of hydrated Zn^{2+} for the high Zn redox kinetics and side reaction alleviation. Moreover, the weak affinity of fly ash with Zn(002) plane than with Zn(100) and Zn(101) planes enables a planar deposition of Zn^{2+} on the Zn anode surface during Zn deposition process, which realizes homogeneous and dendrite-free Zn anodes.

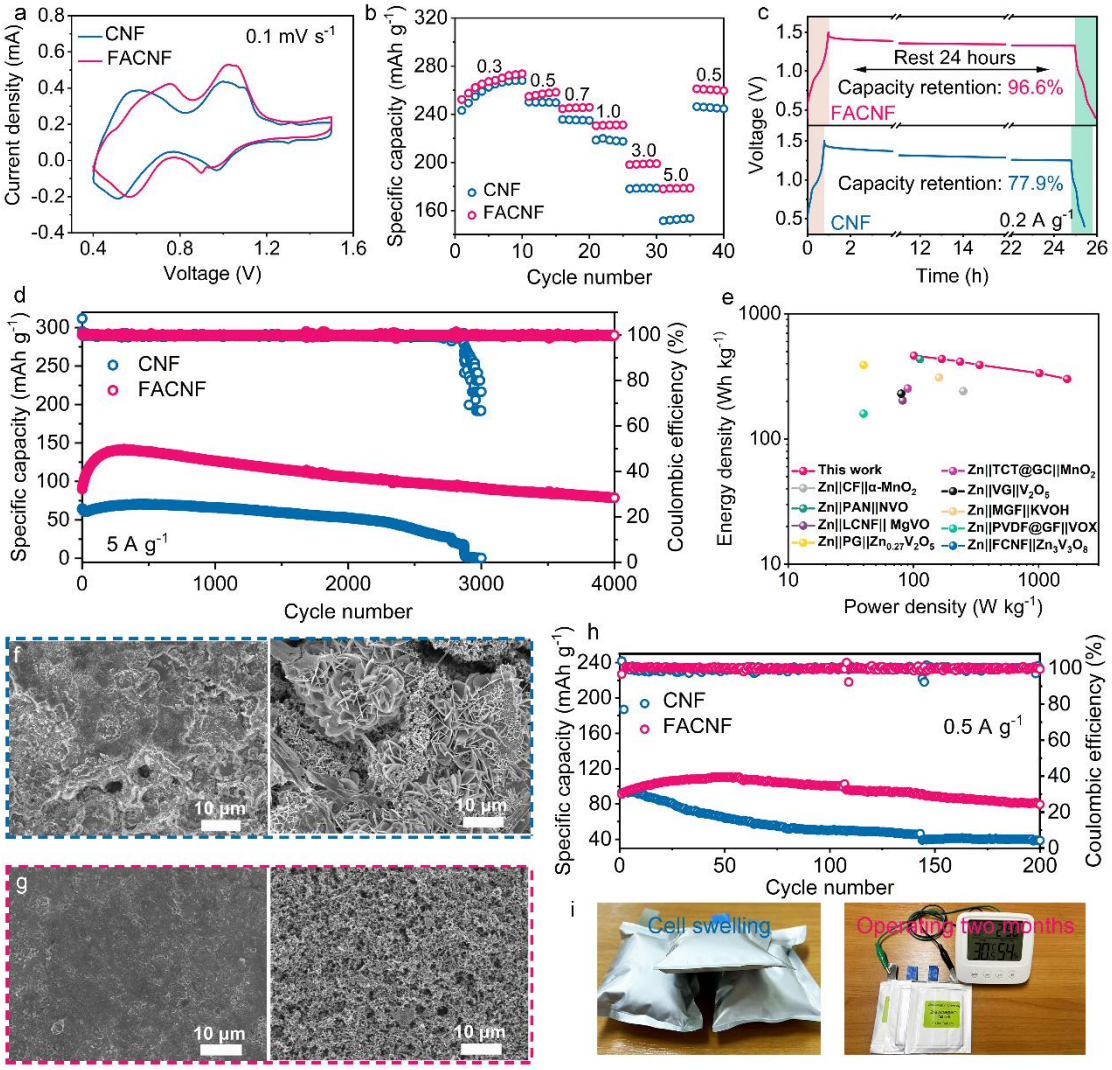

Figure 5. (a) CV curves of Zn||NVO full cells with CNF and FACNF separators tested at the scan rate of 0.1 mV s^{-1}. (b) Rate performances of Zn||NVO full cells with CNF and FACNF separators. (c) Capacity retention of Zn||NVO full cells after rest 24 h. (d) Long-term cycling performances of Zn||NVO full cells tested at the current density of 5 A g^{-1}. (e) Comparison of Ragone plots. SEM images of Zn anodes and NVO cathodes in the full cell with (f) CNF and (g) FACNF separators after 1000 cycles. (h) Cycling stabilities of Zn||NVO pouch cells. (i) The digital photographs of Zn||NVO pouch cells with CNF and FACNF after operation.

The full cells using NVO materials as the cathode were assembled to ascertain the reliability and practicability of FACNF separator in AZIBs. The XRD pattern and SEM images of NVO material are shown in Figures S11 and S12. The SEM image of NVO on carbon paper is shown in Figure S13. In the CV curves (Figure 5a), the Zn||NVO

full cell using FACNF separator shows stronger current density and smaller voltage polarization between the redox peaks than using CNF separator, mainly attribute to the promoted desolvation process of hydrated zinc ions and charge transfer capability.[54] Figure 5b shows the rate performances of full cells under the various current densities from 0.3 to 5 A g^{-1}. The full cell with FACNF separator delivery higher discharge specific capacity, especially at the high current density of 5 A g^{-1}, resulting from the confined side reactions and minimal charge transfer resistance enabled by FACNF separator. This can be testified by the EIS plots (Figure S14) that the full cell with FACNF separator shows smaller battery resistance both before and after charge-discharge cycling compared with CNF separator. The energy storage performances of full cells with different separators were monitored to investigate the self-discharge behavior. As shown in Figure 5c, after rested 24 h, the full cell with FACNF separator generates a higher capacity retention of 96.6% than with CNF separator (77.9%), suggesting the enviable ability of FACNF separators in preventing water-induced side reactions. By virtue of the electrochemical superiority of the FACNF separator, the Zn||NVO full cell with the FACNF separator delivers excellent long-term cycling stability with the specific capacity of 79.0 mAh g^{-1} and capacity retention of 92.1% after 4,000 cycles at 5 A g^{-1} (Figure 5d). In comparison, owing to the severe side reactions and dendrite growth, the full cell with CNF separator shows not only low discharge capacity but also the abrupt battery failure around 2,800 cycles. Noting that, the Zn||NVO full cells with CNF and FACNF separators show a discharge tendency that rises first and then slowly decreases, due to the increased active sites of NVO cathode in the initial cycling process and the inherent dissolution in the aqueous solution.[55, 56] Also, the full cell with FACNF separator represents the energy density of 414.5 Wh kg^{-1} and power density of 236.2 W kg^{-1}, overpassing other energy storage systems with the state-of-the-art separators.[19, 21, 22, 29, 57-61] The morphologies of Zn anode and NVO cathode after 1,000 cycles were observed to further demonstrate the superiority of FACNF separator in AZIBs. For the utilization of CNF separator in full cells, serious surface corrosions, pit points and Zn dendrites can be found on the Zn anode, meanwhile the NVO cathode adheres rich Zn nanosheets (Figure 5f), which are the key

factors leading to battery failure. In contrast to that, the FACNF separator in full cell yields intact surfaces of Zn anode and NVO cathode without surface corrosion, passivation, and Zn dendrites (Figure 5g).

Zn||NVO pouch cells with both CNF and FACNF separators were prepared to further verify the viability of using FACNF as the separator in AZIBs. The Zn||NVO pouch cell with FACNF exhibits a steady voltage of 1.2 V under different bent, folded and flat states (Figure S15). As shown in Figure 5h, the pouch cell using FACNF separator exhibits an eminent charge-discharge cycling performance with a discharge capacity of 80.5 mAh g^{-1} and a capacity retention of 87.4% after 200 cycles at discharge current density of 0.5 A g^{-1}, whereas the pouch cell using CNF separator rapidly fade the capacity in the initial 50 cycles and shows low capacity retention of 41.8%. The three-serial pouch cells can power on a thermometer for up to two months without any cell swelling (Figure 5i). In a striking contrast, the pouch cell using CNF shows obvious volume expansion after continuous discharge for one day, indicating that the CNF separator is not qualified for practical applications. These above results manifest that the FACNF separator is a promising candidate for developing stable high-performance AZIBs.

3. Conclusions

In this study, we successfully prepared a low-cost and thermally stable cellulose-based separator filled with fly ash to inhibit dendrite growth and side reactions for Zn anodes. Compared to the CNF separator, the prepared FACNF separator demonstrates higher Zn^{2+} transfer number and ionic conductivity, as well as a lower desolvation energy barrier, which improve the reaction kinetics of Zn^{2+} to Zn^{0} and suppress the possibility of water-induced side reactions. Based on experimental results and theoretical analysis, the FACNF separator effectively guided Zn deposition behavior to preferentially plate Zn(002) plane, resulting in dendrite-free deposition. Benefiting from the high reaction kinetics, dendrite-free deposition behavior and limited side reactions, symmetric and full cells using the FACNF separator exhibit long and stable cycling performance with a dendrite-free electrode surface. Moreover, the pouch cell with the FACNF can operate steadily a digital thermometer for up to two months

without any gas generation and volume expansion. We believe that the developed cellulose-based separator here has great potential as a cost-effective and stable separator for advanced zinc-ion batteries.

Supporting information

Supporting Information is available from

Acknowledgements

This work was supported by the National Natural Science Foundation of China (Grant No. 52125405 and U22A20108), Thailand Science Research and Innovation Fund Chulalongkorn University (INDF67620003), National Science, Research and Innovation Fund (NSRF) via the Program Management Unit for Human Resources & Institutional Development, Research and Innovation (Grant No. B05F640153), and National Research Council of Thailand (NRCT) and Chulalongkorn University (N42A660383). C. Yang thanks the support from the Second Century Fund (C2F) scholarship, Chulalongkorn University.

References

[1] Bates, A. M.; Preger, Y.; Torres-Castro, L.; Harrison, K. L.; Harris, S. J.; Hewson, J., *Joule* **2022,** *6* (4), 742-755.

[2] Li, M.; Lu, J.; Chen, Z.; Amine, K., *Adv. Mater.* **2018,** *30* (33), 1800561.

[3] Bayaguud, A.; Luo, X.; Fu, Y.; Zhu, C., *ACS Energy Letters* **2020,** *5* (9), 3012-3020.

[4] Li, L.; Jia, S.; Cheng, Z.; Zhang, C., *ChemSusChem* **2023,** *16* (8), e202202330.

[5] Zhang, X.; Li, Z.; Luo, L.; Fan, Y.; Du, Z., *Energy* **2022,** *238*, 121652.

[6] Niu, F.; Mao, Y.; Wang, N.; Feng, Z.; Chen, J.; Ye, L.; Zhang, S.; Bai, Z.; Dou, S., *J. Colloid Interface Sci.* **2024,** *655*, 760-770.

[7] Wang, D.; Li, Q.; Zhao, Y.; Hong, H.; Li, H.; Huang, Z.; Liang, G.; Yang, Q.; Zhi, C., *Adv. Energy Mater.* **2022,** *12* (9), 2102707.

[8] Yang, J.; Yin, B.; Sun, Y.; Pan, H.; Sun, W.; Jia, B.; Zhang, S.; Ma, T., *Nano-Micro Lett.* **2022,** *14* (1), 42.

[9] Peng, M.; Tang, X.; Xiao, K.; Hu, T.; Yuan, K.; Chen, Y., *Angew. Chem. Int. Ed.* **2023,** *62*, e202302701.

[10] Qian, G.; Zan, G.; Li, J.; Lee, S.-J.; Wang, Y.; Zhu, Y.; Gul, S.; Vine, D. J.; Lewis, S.; Yun, W.; Ma, Z.-F.; Pianetta, P.; Lee, J.-S.; Li, L.; Liu, Y., *Adv. Energy Mater.* **2022,** *12* (21), 2200255.

[11] Wang, T.; Li, C.; Xie, X.; Lu, B.; He, Z.; Liang, S.; Zhou, J., *ACS Nano* **2020,** *14* (12), 16321-16347.

[12] Xi, C.; Xiao, Y.; Yang, C.; Li, M.; Li, L.; Chao, Y.; Li, L.; He, C.; Yu, Y., *J. Mater. Chem. A* **2023,** *11* (12), 6522-6529.

[13] Xie, D.; Sang, Y.; Wang, D.-H.; Diao, W.-Y.; Tao, F.-Y.; Liu, C.; Wang, J.-W.; Sun, H.-Z.; Zhang, J.-P.; Wu, X.-L., *Angew. Chem. Int. Ed.* **2023,** *62* (7), e202216934.

[14] Yang, C.; Woottapanit, P.; Cao, J.; Yue, Y.; Zhang, D.; Yi, J.; Zeng, Z.; Zhang, X.; Qin, J.; Wang,

Y., *J. Mater. Chem. A* **2023**.
[15] Wang, G.; Yao, Q.; Dong, J.; Ge, W.; Wang, N.; Bai, Z.; Yang, J.; Dou, S., *Adv. Energy Mater.* **2023**, 2303221.
[16] Lee, B.-S.; Cui, S.; Xing, X.; Liu, H.; Yue, X.; Petrova, V.; Lim, H.-D.; Chen, R.; Liu, P., *ACS Appl. Mater. Inter.* **2018,** *10* (45), 38928-38935.
[17] Zhang, D.; Cao, J.; Chanajaree, R.; Yang, C.; Chen, H.; Zhang, X.; Qin, J., *ACS Appl. Mater. Inter.* **2023,** *15* (9), 11940-11948.
[18] Zhang, Y.; Yang, G.; Lehmann, M. L.; Wu, C.; Zhao, L.; Saito, T.; Liang, Y.; Nanda, J.; Yao, Y., *Nano Lett.* **2021,** *21* (24), 10446-10452.
[19] Li, Y.; Peng, X.; Li, X.; Duan, H.; Xie, S.; Dong, L.; Kang, F., *Adv. Mater.* **2023,** *35* (18), 2300019.
[20] Cao, J.; Zhang, D.; Gu, C.; Wang, X.; Wang, S.; Zhang, X.; Qin, J.; Wu, Z.-S., *Adv. Energy Mater.* **2021,** *11* (29), 2101299.
[21] Su, Y.; Liu, B.; Zhang, Q.; Peng, J.; Wei, C.; Li, S.; Li, W.; Xue, Z.; Yang, X.; Sun, J., *Adv. Funct. Mater.* **2022,** *32* (32), 2204306.
[22] Zhou, J.; Zhang, Z.; Jiang, W.; Hou, S.; Yang, K.; Li, Q.; Pan, L.; Yang, J., *J. Alloys Compd.* **2023,** *950*, 169836.
[23] Guo, G.; Tan, X.; Wang, K.; Zheng, L.; Zhang, H., *J. Power Sources* **2023,** *553*, 232321.
[24] Zhang, X.; Li, J.; Qi, K.; Yang, Y.; Liu, D.; Wang, T.; Liang, S.; Lu, B.; Zhu, Y.; Zhou, J., *Adv. Mater.* **2022,** *34* (38), 2205175.
[25] Liu, Y.; Liu, S.; Xie, X.; Li, Z.; Wang, P.; Lu, B.; Liang, S.; Tang, Y.; Zhou, J., *InfoMat* **2023,** *5* (3), e12374.
[26] Zong, Y.; He, H.; Wang, Y.; Wu, M.; Ren, X.; Bai, Z.; Wang, N.; Ning, X.; Dou, S. X., *Adv. Energy Mater.* **2023,** *13* (20), 2300403.
[27] Li, L.; Peng, J.; Jia, X.; Zhu, X.; Meng, B.; Yang, K.; Chu, D.; Yang, N.; Yu, J., *Electrochim. Acta* **2022,** *430*, 141129.
[28] Li, Y.; Wang, Z.; Cai, Y.; Pam, M. E.; Yang, Y.; Zhang, D.; Wang, Y.; Huang, S., *Energ. Environ. Sci.* **2022,** *5* (3), 823-851.
[29] Fang, Y.; Xie, X.; Zhang, B.; Chai, Y.; Lu, B.; Liu, M.; Zhou, J.; Liang, S., *Adv. Funct. Mater.* **2022,** *32* (14), 2109671.
[30] Zhang, J.; Zhang, S.; Liu, B., *J. Clean. Prod.* **2020,** *250*, 119507.
[31] Zhang, Y.; Wang, L.; Chen, L.; Ma, B.; Zhang, Y.; Ni, W.; Tsang, D. C. W., *J. Hazard. Mater.* **2021,** *411*, 125132.
[32] Yu, K.; Liu, Y.; Jia, M.; Wang, C.; Yang, Y., *J. Energy Storage* **2022,** *51*, 104388.
[33] Li, Y.; Yang, L.; Li, X.; Miki, T.; Nagasaka, T., *J. Hazard. Mater.* **2021,** *411*, 125044.
[34] Ahmaruzzaman, M., *Prog. Energy Combust.* **2010,** *36* (3), 327-363.
[35] Soudais, Y.; Moga, L.; Blazek, J.; Lemort, F., *J. Anal. Appl. Pyrol.* **2007,** *78* (1), 46-57.
[36] Szcześniak, L.; Rachocki, A.; Tritt-Goc, J., *Cellulose* **2008,** *15* (3), 445-451.
[37] Zong, Q.; Lv, B.; Liu, C.; Yu, Y.; Kang, Q.; Li, D.; Zhu, Z.; Tao, D.; Zhang, J.; Wang, J.; Zhang, Q.; Cao, G., *ACS Energy Lett.* **2023,** *8* (7), 2886-2896.
[38] Yang, C.; Zhang, X.; Cao, J.; Zhang, D.; Kidkhunthod, P.; Wannapaiboon, S.; Qin, J., *ACS Appl. Mater. Inter.* **2023**.
[39] Hao, J.; Li, B.; Li, X.; Zeng, X.; Zhang, S.; Yang, F.; Liu, S.; Li, D.; Wu, C.; Guo, Z., *Adv. Mater.* **2020,** *32* (34), 2003021.
[40] Song, Y.; Ruan, P.; Mao, C.; Chang, Y.; Wang, L.; Dai, L.; Zhou, P.; Lu, B.; Zhou, J.; He, Z., *Nano-*

Micro Lett. **2022,** *14* (1), 218.
[41] Zhao, Z.; Zhao, J.; Hu, Z.; Li, J.; Li, J.; Zhang, Y.; Wang, C.; Cui, G., *Energ. Environ. Sci.* **2019,** *12* (6), 1938-1949.
[42] Meng, Z.; Jiao, Y.; Wu, P., *Angew. Chem. Int. Ed.* **2023,** *62* (31), e202307271.
[43] Lin, Y.; Mai, Z.; Liang, H.; Li, Y.; Yang, G.; Wang, C., *Energ. Environ. Sci.* **2023,** *16* (2), 687-697.
[44] Zhao, R.; Wang, H.; Du, H.; Yang, Y.; Gao, Z.; Qie, L.; Huang, Y., *Nat. Commun.* **2022,** *13* (1), 3252.
[45] He, P.; Huang, J., *Adv. Mater.* **2022,** *34* (18), 2109872.
[46] Tian, H.; Yang, J.-L.; Deng, Y.; Tang, W.; Liu, R.; Xu, C.; Han, P.; Fan, H. J., *Adv. Energy Mater.* **2023,** *13* (1), 2202603.
[47] Luo, B.; Wang, Y.; Sun, L.; Zheng, S.; Duan, G.; Bao, Z.; Ye, Z.; Huang, J., *J. Energy Chem.* **2023,** *77*, 632-641.
[48] Zhu, J.; Bie, Z.; Cai, X.; Jiao, Z.; Wang, Z.; Tao, J.; Song, W.; Fan, H. J., *Adv. Mater.* **2022,** *34* (43), 2207209.
[49] Wu, F.; Du, F.; Ruan, P.; Cai, G.; Chen, Y.; Yin, X.; Ma, L.; Yin, R.; Shi, W.; Liu, W.; Zhou, J.; Cao, X., *J. Mater. Chem. A* **2023,** *11* (21), 11254-11263.
[50] Zhang, Y.; Li, X.; Fan, L.; Shuai, Y.; Zhang, N., *Cell Rep. Phys. Sci.* **2022,** *3* (4), 100824.
[51] Zhao, R.; Dong, X.; Liang, P.; Li, H.; Zhang, T.; Zhou, W.; Wang, B.; Yang, Z.; Wang, X.; Wang, L.; Sun, Z.; Bu, F.; Zhao, Z.; Li, W.; Zhao, D.; Chao, D., *Adv. Mater.* **2023,** *35* (17), 2209288.
[52] Deng, R.; He, Z.; Chu, F.; Lei, J.; Cheng, Y.; Zhou, Y.; Wu, F., *Nat. Commun.* **2023,** *14* (1), 4981.
[53] Liu, X.; Lu, Q.; Yang, A.; Qian, Y., *Chinese Chem. Lett.* **2023,** *34* (6), 107703.
[54] Yang, J.-L.; Liu, L.; Yu, Z.; Chen, P.; Li, J.; Dananjaya, P. A.; Koh, E. K.; Lew, W. S.; Liu, K.; Yang, P.; Fan, H. J., *ACS Energy Letters* **2023,** *8* (4), 2042-2050.
[55] Xu, X.; Duan, M.; Yue, Y.; Li, Q.; Zhang, X.; Wu, L.; Wu, P.; Song, B.; Mai, L., *ACS Energy Lett.* **2019,** *4* (6), 1328-1335.
[56] Lu, Y.; Zhu, T.; van den Bergh, W.; Stefik, M.; Huang, K., *Angew. Chem. Int. Ed.* **2020,** *59* (39), 17004-17011.
[57] Yao, L.; Hou, C.; Liu, M.; Chen, H.; Zhao, Q.; Zhao, Y.; Wang, Y.; Liu, L.; Yin, Z.-W.; Qiu, J.; Li, S.; Qin, R.; Pan, F., *Adv. Funct. Mater.* **2023,** *33* (5), 2209301.
[58] Li, C.; Sun, Z.; Yang, T.; Yu, L.; Wei, N.; Tian, Z.; Cai, J.; Lv, J.; Shao, Y.; Rümmeli, M. H.; Sun, J.; Liu, Z., *Adv. Mater.* **2020,** *32* (33), 2003425.
[59] Li, Z.; Ye, L.; Zhou, G.; Xu, W.; Zhao, K.; Zhang, X.; Hong, S.; Ma, T.; Li, M.-C.; Liu, C.; Mei, C., *Chem. Eng. J.* **2023,** *457*, 141160.
[60] Zhou, W.; Chen, M.; Tian, Q.; Chen, J.; Xu, X.; Wong, C.-P., *Energy Storage Mater.* **2022,** *44*, 57-65.
[61] Shen, F.; Du, H.; Qin, H.; Wei, Z.; Kuang, W.; Hu, N.; Lv, W.; Yi, Z.; Huang, D.; Chen, Z.; He, H., *Small* **2023,** *20*, 2305119.

Fly ash particles as industrial waste are introduced into cellulose separators to adjust chemical affinity toward Zn(002) plane and expedite crystallographic homogeneity of Zn anode. The resultant separator can greatly optimize ion transportation kinetics and Zn^{2+} desolvation energy and realize dendrite-free Zn deposition and thus prolong cycling lifespan of symmetric and full cells.

Chengwu Yang[1], Pattaraporn Woottapanit[1], Yilei Yue[1], Sining Geng, Jin Cao, Xinyu Zhang*, Guanjie He*, Jiaqian Qin*

Industrial Waste Derived Separators for Zn-Ion Batteries Achieve Homogeneous Zn(002) Deposition Through Low Chemical Affinity Effects